RSC Advances

ROYAL SOCIETY OF CHEMISTRY

www.rsc.org/advances

Cite this: DOI: 10.1039/cOxxOOOOOx

www.rsc.org/xxxxxx

ARTICLE TYPE

Template-Assisted Synthesis of Multi-Shelled Carbon Hollow Spheres with Ultralarge Pore Volume as Anode Materials in Li-Ion Batteries

Zhuang Sun,[a,b] Xuefeng Song,*[a,b] Peng Zhang[a,b] and Lian Gao*[a,b]

Received (in XXX, XXX) Xth XXXXXXXXX 20XX, Accepted Xth XXXXXXXXX 20XX

DOI: 10.1039/b000000x

By reinventing single-shelled silica hollow spheres and double-shelled silica hollow spheres as the permeable templates, double and quadruple shells carbon hollow spheres are prepared. For this intriguing architecture, the ultralarge pore volume (3.02 $cm^3 g^{-1}$) and the ultrahigh Brunauer-Emmett-Teller (BET) specific surface areas (~1534 $m^2 g^{-1}$) endow the multi-shelled carbon hollow structures with high reversible capacity (~978 mAh g^{-1}). Remarkably, a high capacity of 753 mAh g^{-1} at both low and high current densities can still be attained after 75 cycles. Such a breathable structure makes the multi-shelled hollow structure a superior anode material for a Li-ion battery.

Introduction

For commercial rechargeable lithium ion batteries (LIBs), graphite-based materials are widely used as the traditional anode materials by virtue of their low cost, good electronic conductivity, low and flat electrochemical potential and long cycle life, etc.[1,2] Nevertheless, they are suffered from two main disadvantages, including the limited storage capacity (372 mAh g^{-1}) and the poor rate performance induced by low Li diffusion constant (10^{-6} to 10^{-11} cm^2 s^{-1}).[3,4] To circumvent these issues, hollow structured carbon materials have attracted considerable attention,[5-12] due to the following aspects: 1) the large surface area leads to sufficient electrode/electrolyte interface to absorb Li^+, promoting specific capacity; 2) the ultrathin shell can reduce the transport length of Li^+, while the nanopores on their surface facilitate Li^+ transfer via enormous channels; 3) the hollow interior can buffer against the structure strain associated with the local volume change during charge/discharge and provide extra space for the storage of Li^+. Although a number of achievements have been made, a major challenge for hollow structured carbon active materials still need to be addressed, such as low volume occupying rate ($V_{active\ materials}/V_{total}$), which leads to low content of active materials per unit volume and decreased specific capacity.[13,14]

Very recently, it has been demonstrated that multi-shelled structures can maximize the advantages of hollow nanostructures due to their higher active surface area per unit volume and larger volume occupying rate than that of single-shelled hollow structures, for example, double-shelled Co_3O_4 with volume occupying rate (92%) exhibits higher reversible specific capacity than the single-shelled one with 78% volume occupying rate.[13]Wang et al. and co-workers also confirmed that the triple-shelled Co_3O_4 hollow microspheres exhibit much higher reversible specific capacity (~1615.8 mAh g^{-1}) than the single-shelled one (~792.7 mAh g^{-1}) after 30 cycles.[15] Even at high current density, multi-shelled hollow structures can still retain superior lithium storage capacities, such as multi-shelled SnO_2 hollow microspheres (500 mAh g^{-1} at 1000 mA g^{-1} after 20 cycles)[16] and double-shelled $CoMn_2O_4$ hollow microcubes (406 mAh g^{-1} at 800 mA g^{-1} after 50 cycles).[17] The significantly better electrochemical performance for multi-shelled hollow spheres is mainly attributed to the following two factors: 1) the increased porosity of the shells and the interior cavities lead to an increase in electrolyte/materials contact area and a decrease in the effective diffusion distance for both lithium ions and electrons.[15] 2) the volume occupying rate reaches its optimized value, which will increase the energy density by increasing the weight fraction of the electrochemical active component.[13, 18] However, most of the methods to achieve this special nanostructure are only suitable for specific metal oxides,[13,15-17,19,20] and cannot be applied to other materials such as carbon materials, which is a fundamental challenge for synthetic chemistry owing to complicated structure and difficulty in accessibility of proper templates. For both technical and environmental reasons, multi-shelled carbon hollow structures are highly desirable, and can be regarded to hold the promise for improving the properties of materials. However, it is very difficult to obtain desirable hollow templates for creating multi-shelled hollow structures, since it requires that the shell of the template contains transverse channels to allow the precursors to penetrate and effective coating on both inner and outer surfaces of the shell.[21]

State Key Lab of Metal Matrix Composites
School of Materials Science and Engineering
Shanghai Jiao Tong University
800 Dongchuan Rd.
Shanghai, P. R. China 200240
Fax:+86-21-52413122; Tel: +86-21-52412718
E-mail: liangao@mail.sic.ac.cn, songxfeng@sjtu.edu.cn

Electronic Supplementary Information (ESI) available: Fig. S1-S8, Scheme S1 and Table S1. See DOI: 10.1039/b000000x/

Recent studies suggest that the high specific surface area and pore volume are desirable for enhanced electrochemical performance of hollow carbon structures, which not only facilitate ion transport by short diffusion pathway and easy accessibility of electrolyte, but also provide higher surface density of actives sites by increasing the exposed area. Abundant cavities, large numbers of pores and hollow structures in the electrode materials contribute to the high pore volume and would serve as reservoirs for the storage of Li^+, improving the electrochemical properties of samples.[22,23] Open pores in electrode materials can also allow the diffusion of Li^+ from outside carbon into the inner carbon, which activates all the carbon material.[22] For example, Zhang et al.[24] reported a double-shelled hollow carbon/sulfur sphere with a high surface area of 748 m^2 g^{-1} and pore volume up to 1.69 cm^3 g^{-1} shows extraordinary electrochemical performance. Other porous carbon based hollow structures, such as hollow carbon nanotube/carbon nanofiber hybrid[22] and interconnected hollow carbon nanospheres[7] as well as nanographene constructed hollow carbon spheres[25], have shown the high surface area and large pore volume benefiting the enhanced electrochemical performances. Unfortunately, although many achievements have been obtained, the synthesis of hollow carbon structures with both an ultrahigh surface area up to 1500 m^2 g^{-1} and ultralarge pore volume up to 2.5 cm^3 g^{-1} still remains a huge challenge. Moreover, the most of previous reported hollow carbon structures achieved micrometer level porosity. For electrochemical applications, carbon materials with mesopores can provide short mass diffusion distance and high interface area between the electrolyte and electrode, delivering enhanced electrochemical performances, such as ordered mesoporous carbon[26] and hierarchically porous carbon.[27] To further improve the performance of hollow carbon based materials for LIBs, a facile and efficient method to synthesize carbon hollow spheres with ultrahigh surface area and ultralarge pore volume is highly desirable."

Herein, we report the controllable synthesis of novel multi-shelled carbon hollow spheres (including double-shelled, quadruple-shelled structures) under the assistance of permeably mesoporous silica hollow spheres (MSHS). We reinvent a novel MSHS template containing controlled number of SiO_2 shell and transverse channels in the shell, which can readily manipulate the number of subsequent carbon shells. To the best of our knowledge, this is the first report on fabricating multi-shelled carbon hollow spheres as anode materials for LIBs. For this intriguing architecture, the ultralarge pore volume (3.02 cm^3 g^{-1}) and the ultrahigh Brunauer-Emmett-Teller (BET) specific surface areas (~1534 m^2 g^{-1}) endow the multi-shelled carbon hollow structures with more lithium storage sites, which delivers the excellent capacity; Meanwhile, a short transport path for both Li^+ and e^- diffusion resulting from porous ultrathin shells (~6 nm) and a high Li^+ flux across the interface coming from large electrode-electrolyte contact area, leading to a better rate capability. Moreover, the flexible multishells and sufficient void space in the hollow structure can effectively keep the integrity of the whole electrode, improving the cycling performance.

Experimental Section

Preparation of MSHS: Lauryl sulfonate betaine (LSB) and sodium dodecyl benzenesulfonate (SDBS) were mixed at 1:1 molar ratio and dissolved in deionized water (50 mM) at 40 °C, followed by addition of 60 ul 3-aminopropyltriethoxysilane (APTES) and 600 ul tetraethyl orthosilicate (TEOS), then the mixture was stirred for 1 hour. The above suspension was then placed in water bath at 80 °C for another 20 h to ensure complete polymerization of the silica. The resultant product was obtained after centrifugation, washing with ethanol and water, respectively, and then dried in air at 353 K. To remove the surfactants, the obtained solid was dispersed in the acetonitrile solution containing ~35% HCl while vigorously stirring at room temperature for 4 h and then dried at 60 °C for 12 h to obtain the MSHS.

Preparation of double-shelled silica hollow sphere (DMSHS): LSB and SDBS were mixed at 1:1 molar ratio and dissolved in deionized water, followed by magnetic stirring for 1 h at room temperature; Then, 10 ml MSHS colloidal aqueous solution (10 g L^{-1}) was added into the surfactant mixture (the concentration of LSB/SDBS: 20 mM). After vigorous stirring for another 15 min, the resulting solution was heated in water bath at 40 °C, followed by addition of 50 ul 3-aminopropyltrie-thoxysilane (APTES) and 300 ul tetraethyl orthosilicate (TEOS), and then the mixture was stirred for 1 hour. The above suspension was then placed in water bath at 80 °C for another 20 h to ensure complete polymerization of the silica. The resultant product was obtained after centrifugation, washing with ethanol and water, respectively, and then dried in air at 353 K. To remove the surfactants, the obtained solid was dispersed in the acetonitrile solution containing ~35% HCl while vigorously stirring at room temperature for 4 h and then dried at 60 °C for 12 h to obtain the DMSHS.

Synthesis of multi-shelled carbon hollow spheres: The obtained MSHS or DMSHS (0.1 g) was mixed with glucose (0.5 g) in 10 ml deionized water and stirred for 0.5 hr. The mixture was placed in a 20 ml Teflon-sealed autoclave and maintained at 180 °C in an oven for 4h. The as-prepared product was centrifuged and washed with ethanol and water for 4 times and then dried in air at 80 °C. Finally, the powders were placed in a tube furnace and annealed at 800 °C for 4 hr under argon atmosphere with a heating rate of 4 °C min^{-1}. The silica template was etched using dilute HF solution for 6 hr, and followed by washing with deionized water, to produce multi-shelled carbon hollow spheres.

Characterization: The crystal structure of the as-prepared samples were characterized using powder X-ray diffraction (XRD) on a Goniometer Ultima IV (185 mm) diffractometer with Cu Kα radiation (λ=1.5418 Å) at a step of 0.01 ° per second. Transmission electron microscopy (TEM) images were achieved on a JEOL JEM-2010F transmission electron microscope operated at an acceleration voltage of 200 kV. Morphologies of as-obtained products were observed on a field emission scanning electron microscopy (FESEM, FEI Sirion 200). Nitrogen adsorption and desorption measurements were performed with an Autosorb iQ instrument. The surface areas were calculated by the Brunauer-Emmett-Teller (BET) method, and the pore size distribution was calculated from the adsorption isotherm curves using density functional theory (DFT) method. Raman spectra were taken on a DXR Raman Microscope with an excitation length of 532 nm. Thermal gravimetric analysis (TG) was

Cite this: DOI: 10.1039/cOxxOOOOOx
www.rsc.org/xxxxxx

ARTICLE TYPE

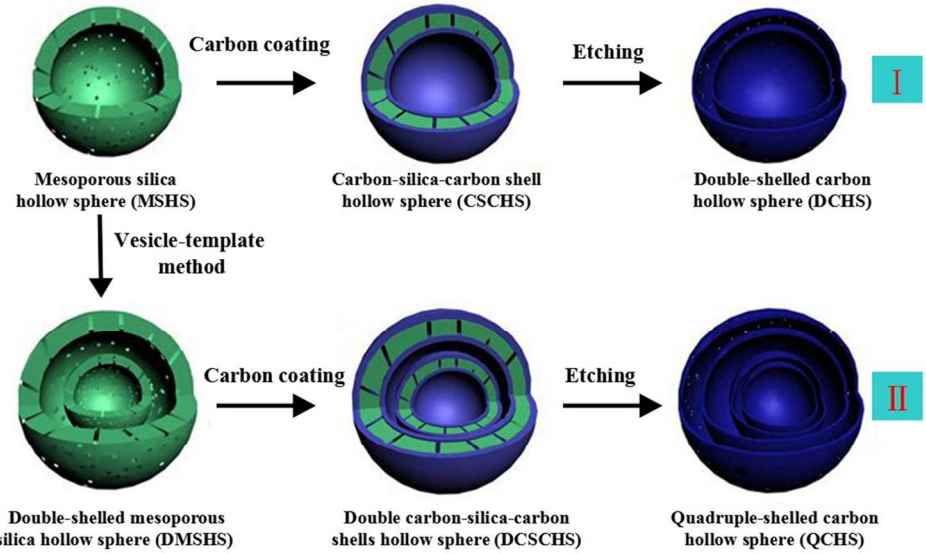

Scheme 1. Schematic illustration for producing double/quadruple-shelled carbon hollow spheres. Step I and II present the permeable template-assisted synthesis of double-shelled carbon hollow sphere and quadruple-shelled carbon hollow sphere using single-shelled silica hollow sphere (MSHS) or double-shelled silica hollow sphere (DMSHS) as template, respectively.

conducted on a PE TGA-7 instrument with a heating rate of 20 °C min^{-1}.

Electrochemical characterization: For preparing working electrodes, a mixture of the as-fabricated samples, carbon black, and poly (vinylidene fluoride) (PVDF) at a weight ratio of 6:2:2 was put in N-methyl-2-pyrrolidoner (NMP) solvent to form a slurry, which was then pasted on a copper foil (Shenzhen Kejing Star Technology Co., China). After drying in vacuum at 80 °C, the electrodes were tested in coin cells with Li metal as counter and reference electrodes. The electrolyte was 1 M LiPF6 in a mixture solution of ethylene carbonate (EC), diethyl carbonate (DEC) and ethyl methyl carbonate (EMC) in a 1:1:1 volume ratio (Shenzhen Kejing Star Technology Co., China). A microporous membrane (Celgard 2400) was used as the separator. The coin cells were assembled in an argon filled glove box. The galvanostatic charge-discharge tests were conducted in a voltage interval of 0 V to 3 V using a Bio-Logic VMP-300 Battery Testing System at room temperature. The specific capacity of the multi-shelled carbon hollow spheres electrode was calculated by using the mass of multi-shelled carbon hollow sphere nanohybrids.

Results and Discussion

The synthesis of double-shelled carbon hollow spheres (DCHS) under the assistance of MSHS is illustrated in Step I (Scheme 1). Briefly, the MSHS with diameter ranging from 90~120 nm (as shown in Figure 1a,b) were firstly synthesized using a facile vesicle-template approach previously reported by us.[28] MSHS have good dispersivity and the pore size of which was centered at approximately 3.9 nm examined by the DFT pore size distribution (Figure S1 in the Supporting Information). Secondly, the amino-terminated MSHS were uniformly coated with glucose-derived polysaccharide layer on both the interior and exterior surfaces under hydrothermal condition. The as-prepared carbon-silica-carbon hollow spheres (CSCHS) still show excellent dispersibility and uniform shape (Figure 2a). Figure 2b confirms the CSCHS with carbon-SiO_2-carbon tandem shell. Afterwards, an annealing process under argon atmosphere results in the carbonization of the polysaccharide component. Finally, the SiO_2 shell could be easily dissolved in HF acid to generate double-shelled carbon hollow spheres (DCHS) (Figure 1c, d). The interstice distance between the two carbon shells (5~10 nm) is well consistent with the shell thickness of MSHS (Figure 1a, inset). In order to synthesize the quadruple-shelled carbon hollow spheres (QCHS), the template of DMSHS were first synthesized via repeating the vesicle-template approach with the MSHS as core (Figure 2c).[29] Repeated with the hydrothermal pyrolysis reaction of glucose, step II could produce QCHS with four layer carbon shells after the themolysis of as-obtained product followed by selective etching of SiO_2 shell. From Figure 2d, four layer of carbon shell with diameter of ~6 nm can be evidently observed. TEM images (Figure 1e, Figure S2a) confirm the presence and distribution of quadruple carbon shells, in which one DCHS is encapsulated by the other DCHS, forming a unique DCHS@DCHS "yolk-shell" structure (Figure 1e, inset). From SEM images of multi-shelled carbon hollow spheres (Figure 1d, f), the size of the QCHS (140~170 nm) is bigger than that of the

Cite this: DOI: 10.1039/cOxxOOOOOx
www.rsc.org/xxxxxx

ARTICLE TYPE

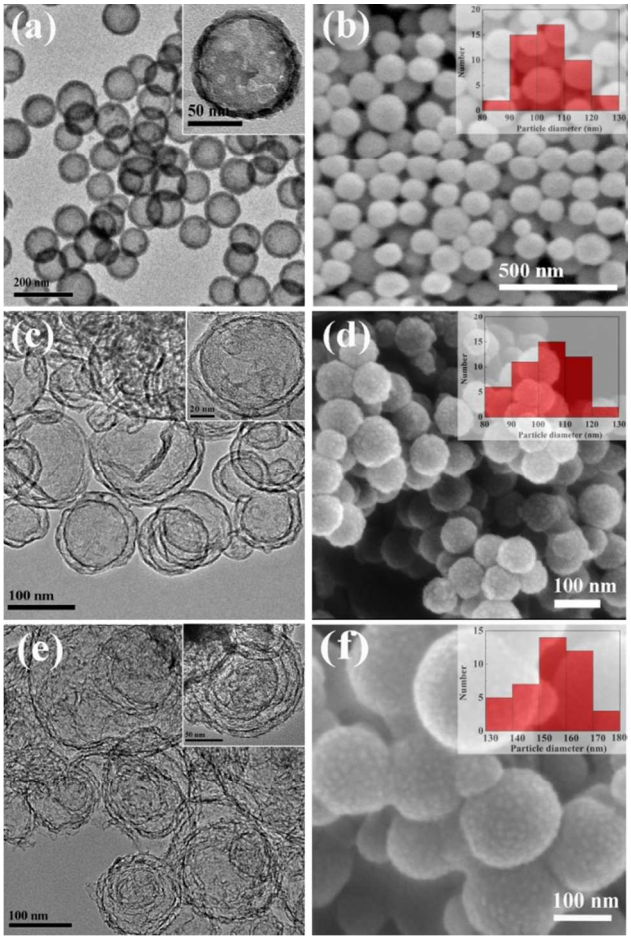

Figure 1. The TEM images and SEM images of MSHS (a, b), DCHS (c, d) and QCHS (e, f), respectively.

DCHS (90~120 nm), owing to their different template size. Additionally, it is obvious that multi-shelled hollow spheres are neatly linked with each other via the carbon shell. Examination of the carbon shells by high-resolution transmission electron microscopy (HRTEM) exhibits that the neighboring shells are interconnected by "carbon bridges" resulted from the carbonization of polysaccharide in the transverse channels in the shells (as evidenced in Figure S2), which ensures continuous electron transport in these structures. It should be noticed that amino-functionalizationed of silica template turns out to be crucial to obtain uniform carbon coating layer without the formation of bare polysaccharide particles.[30] The presence of APTES on the surface of MSHS can be corroborated by the FT-IR spectrum of MSHS (Figure S3), which shows characteristic bands for aliphatic C-H stretching vibration at 3000-2800 cm^{-1}, N-H bending vibration around 690 cm^{-1}, -NH- deformation vibration at 1509 cm^{-1} and NH stretching vibration at 3000-3300 cm^{-1}.[31]

To demonstrate the possible structural advantages of multi-shelled carbon spheres, single-shelled carbon hollow spheres (SCHS) were also prepared for comparison (Figure S4a, b). As we all know, a large surface area associated with structural features of hollow spheres plays key role to improve the electrochemical performance. The specific surface areas for three types of samples can be determined by the adsorption uptake at low relative pressure in the nitrogen adsorption-desorption isotherm (Figure 3a, b, Figure S4c). Three types of hollow carbon spheres exhibit typical IV hysteresis loop at a relative pressure P/P_0 between 0.4 and 1. After carbonization at high temperature, the BET surface area is calculated to be 644.35 $m^2 g^{-1}$, 1004.17 $m^2 g^{-1}$ and 1533.53 $m^2 g^{-1}$ for SCHS, DCHS and QCHS, respectively. To further analyze the pore structures of three types of hollow carbon spheres, the pore size distribution were obtained by quenched solid density functional theory (QSDFT) model for characterization of carbon using nitrogen adsorption. It is evident that the QCHS possess more broader mesoporous peaks than both SCHS and DCHS, expect that micropores centered around 1.35 nm, indicating the presence of higher surface area and pore volume in the QCHS. Surprisingly, the QCHS displays an ultrahigh pore volume of 3.02 $cm^3 g^{-1}$. This pore volume is much higher than that of DCHS (1.79 $cm^3 g^{-1}$) and SCHS (0.29 $cm^3 g^{-1}$), which is even larger than the most reported nanostructured carbon such as hollow carbon nanotube/carbon nanofiber hybrid with 1.21 $m^3 g^{-1}$,[22] tube-in-tube structured carbon with 1.77 $m^3 g^{-1}$ [32] and other carbon hybrid structures (Table S1). The ultrahigh pore volume could be partly attributed to a large amount of microporous structures (0.40 $cm^3 g^{-1}$ for DCHS and 0.61 $cm^3 g^{-1}$ for QCHS) such as defects and cavities on the surface of carbon

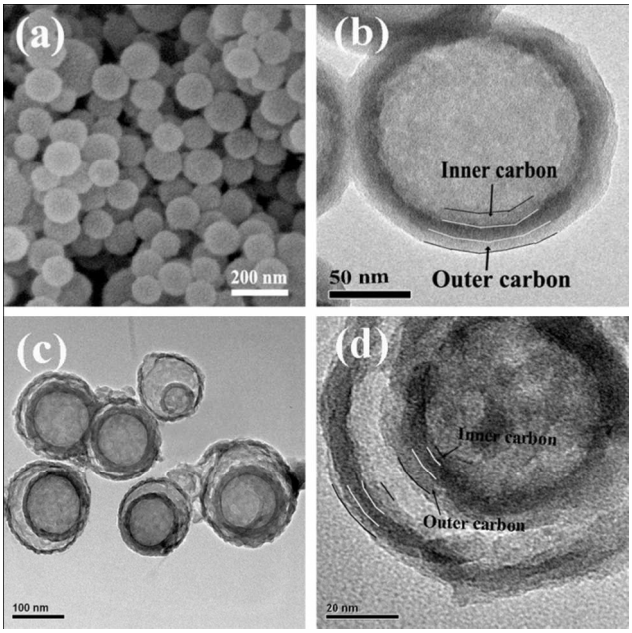

Figure 2. The SEM image of (a) CSCHS. The TEM images of (b)CSCHS, (c) DMSHS and (d) DCSCHS.

Cite this: DOI: 10.1039/cOxxOOOOOx

www.rsc.org/xxxxxx

ARTICLE TYPE

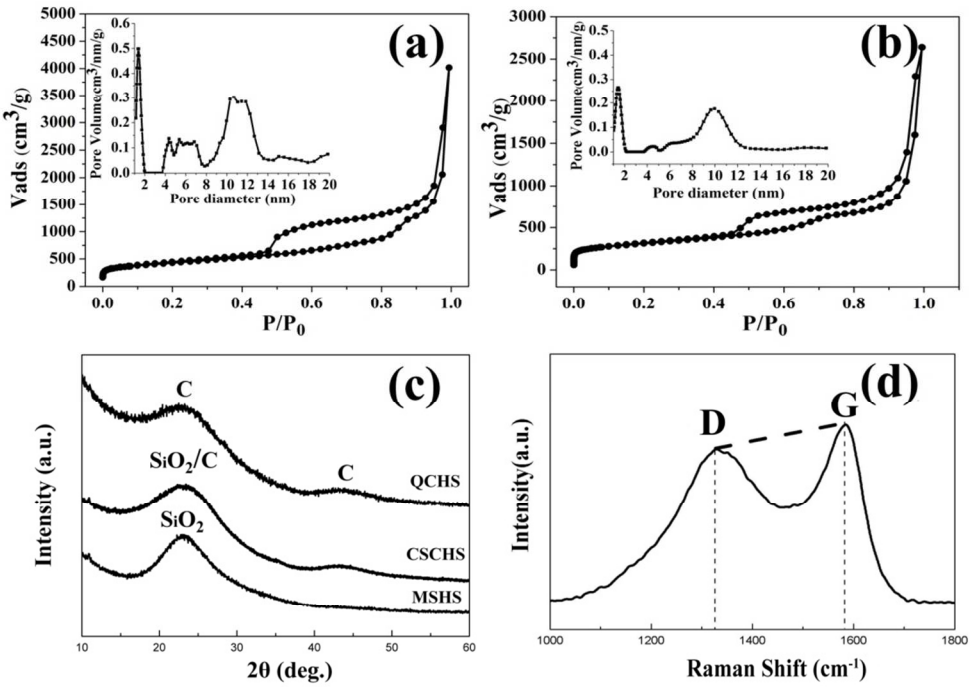

Figure 3. Nitrogen adsorption-desorption isotherms with corresponding pore size distributions (inset) of QCHS (a) and DCHS (b). c) The XRD patterns of the MSHS, CSCHS and QCHS; d) The Raman spectrum of the QCHS.

sheath originated from carbonization of polysaccharide layer. Furthermore, interspaces at mesoscopic scale between the multishells are also crucial for ultralarge pore volume. The abrupt nitrogen uptake at $P/P_0 > 0.8$ in the nitrogen adsorption-desorption isotherms for QCHS and DCHS revealed the textural porosity between the nanoparticles as well as internal hollow space of each nanoparticle, which can be calculated at p/p_0=0.99~0.8 (1.35 $cm^3\ g^{-1}$ for QCHS and 0.82 $cm^3\ g^{-1}$ for DCHS).[33] The XRD patterns of the MSHS, CSCHS and QCHS are presented in Figure 3c. It is evident that the MSHS have the broad band at around 23° resulted from amorphous silica; However, the XRD patterns of CSCHS presented two broad diffraction peaks centered at 23° and 43°, indicating the presence of disordered carbon.[34] After complete etching of SiO_2 templates, confirmed by EDS analysis (Figure S5a), the two typical peaks come from carbon only can be observed. The Raman spectrum further confirms typical characteristics of disordered carbon of QCHS, and the I_D/I_G intensity ratio of 0.9 indicates that the carbon layer exhibits a reasonable degree of graphitization (Figure 3d).[35] According to thermogravimetric analysis (TGA) of pristine silica templates (MSHS and DMSHS) and intermediates (CSCHS and DCSCHS), the carbon content in the intermediate CSCHS and DCSCHS can be determined as 24.3 wt% and 32.6 wt% by subtracting the weight loss of silica templates at 900 °C (Figure S5b), indicating that the intermediate DCSCHS contain more carbon than the CSCHS.

The electrochemical behavior of the multi-shelled hollow carbon nanospheres were characterized by cyclic voltammetry at a scan rate of 0.1 mV s^{-1}. Figure 4a shows a typical cyclic voltammogram (CV) curves of the QCHS. In the first cycle, the voltammogram shows a broad cathodic peak at 0.5~0.8 V, which appears only in the first cycle and is related to the formation of a solid electrolyte interphase (SEI) film.[7] However, this peak disappears in the subsequent cycles, suggesting a large initial irreversible capacity after the first cycle. The charge/discharge profiles, as shown in Figure 4b, were generally in agreement with the CV results. During the first cycle, the voltage drops quickly and forms a plateau at 0.5~0.8 V, corresponding to the cathodic peak in CV curve. The first charge capacity is as high as 1254 mAh g^{-1}, nearly four times higher than the theoretical one of graphite (372 mAh g^{-1}) and is also higher than that of other hollow carbon spheres.[7,12,36] Meanwhile, a large irreversible capacity is demonstrated over the first cycle, which is common for carbonaceous materials due to the reduction of the electrolyte on the electrode/electrolyte interface and irreversible interaction between lithium with cavity or residual H atoms.[7,8,10,37] After the first cycle, the irreversible capacity becomes very low, and Coulombic efficiency is very high, which

Cite this: DOI: 10.1039/cOxxOOOOOx
www.rsc.org/xxxxxx

ARTICLE TYPE

is over 98.4 % after 15 cycles (Figure S6a). The specific capacity of QCHS is evidently higher than the theoretical capacity of graphitic carbon (372 mAh g^{-1}), suggesting the existence of other lithium storage mechanisms for QCHS apart from the classical graphite intercalation compound (GIC) mechanism.[38,39] The differential capacity versus cell voltage plots of QCHS (Fig. S6b) exhibit three peaks at ~0.2 V, ~1.4 V and ~2.4 V as well as a slope from 2.7 to 3.0 V, demonstrating that multiple Li storage positions are present in the as-obtained QCHS. The peak at ~0.2 V can be attributed to the Li extraction from the graphitic layers,[22] and the peak at ~1.4 V is ascribed to the Li extraction from the defects in the QCHS, such as pores, vacancies, edges and corners of the graphitic layers, which is similar to that of other hollow carbon spheres and traditional mesoporous carbons.[27,40] The peak at ~2.4 V can be ascribed to the extraction of Li ions bonded with the surface functional groups in the QCHS, which was also observed in the multi-walled carbon nanotubes.[41,42] As has been reported, the slope from 2.7 to 3.0 V is related to the residual H atoms on the surface of QCHS.[25,36] Thus, we can conclude that the existence of multiple lithium-storage positions in QCHS gives rise to very-high reversible capacity. The QCHS also possess both ultralarge pore volume and ultrahigh surface area, which likely provide rich active sites for trapping more Li^+ and accelerate accessibility of electrolyte by strengthened diffusion, substantially delivering the highest initial specific capacity (2495.8 mAh g^{-1}) compared with the DCHS (1745.7 mAh g^{-1}, Figure S6c) and SCHS (759.6 mAh g^{-1}, Figure S6d).

The cycling performance of all multi-shelled hollow carbon spheres are examined at a current density of 50 mA g^{-1} (Figure 4c), wherein QCHS show the highest specific capacity and best cycling performance. After 40 cycles at a current density of 50 mA g^{-1}, the specific capacity of single-, double- and quadruple-shelled carbon nanospheres remained as high as 303.5, 712.1, and 977.6 mAh g^{-1}, respectively. The superior cycling performance of QCHS compared with DCHS and SCHS may be related to different volume occupying rate of the different hollow sphere types. Based on our approximate calculation on carbon multi-shelled hollow spheres (see Supporting Information), the value of volume occupying rate is about 27 %, 47 % and 55 % for SCHS, DCHS and QCHS, respectively. The values of double- and quadruple-shelled hollow spheres are much higher than that of single-shelled hollow spheres, which benefits to obtain high lithium storage capacity. When the carbon shell is inserted by Li ions, there would be around 20 % volume expansion,[43] so the carbon occupies ~66 % of the total space in the QCHS after Li insertion. The void space in QCHS can right accommodate the

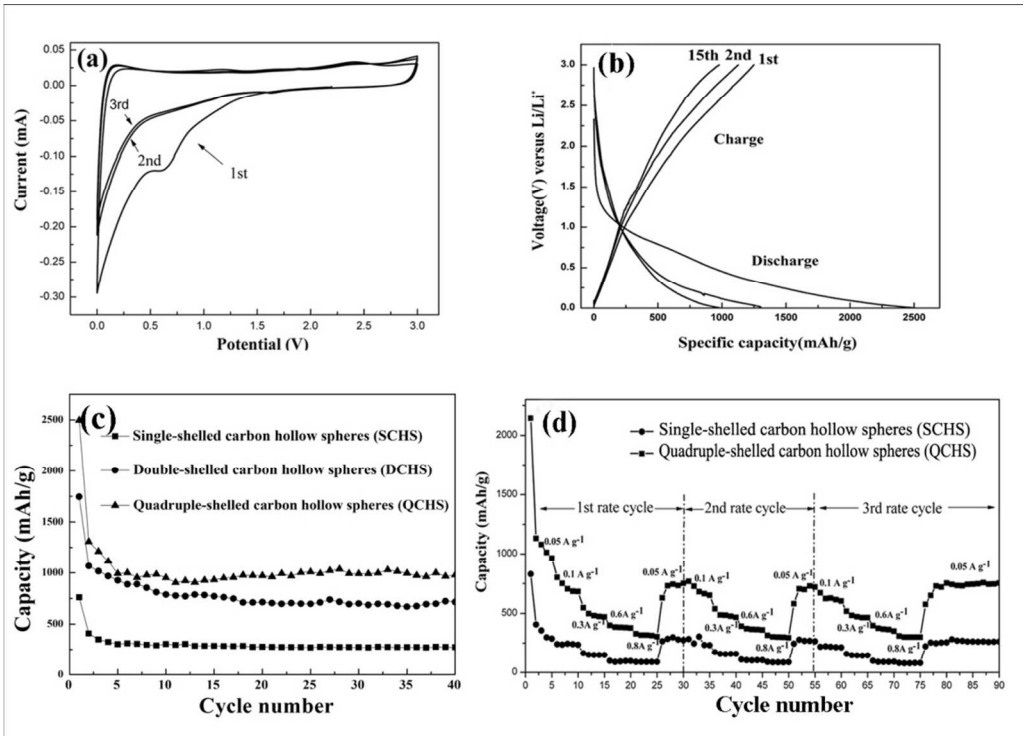

Figure 4. a) Cyclic voltammetry curves of the QCHS, showing the first three cycles between 3.0 V and 0 V at a scan rate of 0.1 mV s^{-1}. b) Galvanostatic charge/discharge curves of QCHS at a current density of 50 mA g^{-1}. c) Discharge capacities versus cycle number for the SCHS, DCHS and QCHS at a current density of 50 mA g^{-1}. d) Rate capabilities of the QCHS and SCHS cycled at various current density from 50 to 800 mA g^{-1}.

Cite this: DOI: 10.1039/cOxxOOOOOx
www.rsc.org/xxxxxx

ARTICLE TYPE

volume after expansion (illustrated in Scheme S1), which ensures the good cycle performance as well as high volume energy density.[13,14] TEM analysis of the multi-shelled hollow carbon nanosphere electrodes after 20 cycles (Figure S8a,b) at a 50 mA g^{-1} demonstrates that the integrity of multi-shelled hollow structures are clearly retained, indicating good cycle stability of both QCHS and DCHS. It should be noted that the shell thickness increased to ~15 nm probably due to the formation of the SEI film,[7] although no clear interface between the original carbon and the SEI film can be observed.

Since the rate capacity is also crucial for practical applications, the discharge curves at various current densities from 50 to 800 mA g^{-1} were measured for QCHS and SCHS (Figure 4d). Even at a high current density of 800 mA g^{-1}, the quadruple-shelled hollow spheres can still deliver a capacity of 317 mAh g^{-1}, which is much higher than 85 mAh g^{-1} observed for the single-shelled hollow spheres, indicating that the unique design of multi-shelled hollow structure plays a key role in improving the rate capacity of carbon materials.[13] Remarkably, a high capacity of 753 mAh g^{-1} at both low and high current densities can still be attained after 75 cycles, when the current density is decreased to 50 mA g^{-1}. Such a "breathable" nature is due to affluent hollow space and elastic buffering shells in this novel nanoarchitecture.[44] The enhanced rate capacity likely attribute to the improved Li^+ and e^- transport and large electrode/electrolyte contact area.

The exceptional electrochemical performance of multi-shelled hollow carbon spheres can be attributed to synergetic effect of ultralarge pore volume and surface area, high volume occupying rate and good electrical conductivity. Firstly, the ultralarge pore volume (3.02 cm^3 g^{-1}) and ultrahigh surface area (1533.53 m^2 g^{-1}) resulted from the novel multi-shelled hollow structure, delivers high electrode/electrolyte contact area to trap lithium ions and accelerate the reaction kinetics via very short lithium transport distances, which increases the utilization of active materials and contributes to the high capacity and rate capability.[8,22,27,45] Secondly, optional volume occupying rate of the QCHS, increases the contact surface with the electrolyte, and concurrently provides enough void space to right accommodate the volume change during repetitive cycling, leading to extraordinary cycling performance. Finally, the sufficient void space in the interior and interspace between the shells allow for the elastic carbon shells to expand and contract during repetitive Li^+ insertion-extraction without breaking the integral structure. Such a "breathable" nanoarchitecture is anticipated to offer good cycle life and excellent rate performance.[44] Moreover, the inter-connected carbon spheres and the inter-spaced carbon bridges provide continuous electron transport pathway in the whole electrode, further ensuring the improved rate performance.

Conclusions

In summary, unique multi-shelled carbon hollow spheres were successfully synthesized by permeable SiO_2 template with mesoporous features. By adjusting the structures of the templates, the number of carbon shells can be accurately controlled. The superior performance in LIBs originates from the porous hollow multi-shelled microstructure, which guarantees more lithium-storage sites, shorter lithium-ion diffusion lengths and sufficient void space to buffer the volume expansion. By comparison, the QCHS with 1533.53 m^2 g^{-1} of superhigh specific surface area and 3.02 cm^3 g^{-1} of ultralarge pore volume exhibit superior electrochemical results, and where specific capacity approaches 978 mAh g^{-1} over 40 cycles, meanwhile keeping good cycling performance and excellent rate performance. Our results show that the multi-shelled carbon hollow spheres are promising anode materials for the next-generation LIBs with excellent electrochemical performance. Furthermore, we believe that the obtained multi-shelled carbon hollow spheres may also be applicable for supercapacitor, biomaterials, catalyst and hydrogen storage.

Acknowledgements

The authors greatly acknowledge the financial support by the Shanghai Municipal Natural Science Foundation (12ZR1414300), the National Natural Science Foundation of China (51302169, 51172142), and the Third Phase of 211 Project for Advanced Materials Science (WS3116205006, WS3116205007).

Notes and references

1 L. W. Ji, Z. Lin, M. Alcoutlabi and X. W. Zhang, *Energy Environ. Sci.*, 2011, **4**, 2682.
2 Y. Weng, Z. S. Feng, J. J. Chen, C. Zhang, X. Jin, J. Hu, *Solid State Commun.*, 2012, **152**, 1577.
3 K. Persson, V. A. Sethuraman, L. J. Hardwick, Y. Hinuma, Y. S. Meng, A. V. D. Ven, V. Srinivasan, R. Kostecki and G. Ceder, *J. Phys. Chem. Lett.*, 2010, **1**, 1176.
4 Z. G. Yang, J. L. Zhang, M. C. W. Kintner-Meyer, X. C. Lu, D. Choi, J. P. Lemmon and J. Liu, *Chem. Rev.*, 2011, **111**, 3577.
5 K. X. Wang, Z. L. Li, Y. G. Wang, H. M. Liu, J. S. Chen, J. Holmes and H. S. Zhou, *J. Mater. Chem.*, 2010, **20**, 9748.
6 J. Liu, W. Liu, K. F. Chen, S. M. Ji, Y. C. Zhou, Y. L. Wan, D. F. Xue, P. Hodgson and Y. C. Li, *Chem. Eur. J.*, 2013, **19**, 9811.
7 K. Tang, R. J. White, X. K. Mu, M. M. Titirici, P. A. van Aken and J. Maier, *ChemSusChem*, 2012, **5**, 400.
8 L. Qie, W. M. Chen, Z. H. Wang, Q. G. Shao, X. Li, L. X. Yuan, X. L. Hu, W. X. Zhang and Y. H. Huang, *Adv. Mater.*, 2012, **24**, 2047.
9 B. S. Lee, S. B. Son, K. M. Park, W. R. Yu, K. H. Oh and S. H. Lee, *J. Power Sources*, 2012, **199**, 53.
10 L. G. Bulusheva, A. V. Okotrub, A. G. Kurenya, H. K. Zhang, H. J. Zhang, X. H. Chen and H. H. Song, *Carbon*, 2011, **49**, 4013.
11 J. Liu and D. F. Xue, *Nanoscale Res. Lett.*, 2010, **5**, 1525.

12 F. B. Su, X. S. Zhao, Y. Wang, L. K. Wang and J. Y. Lee, *J. Mater. Chem.*, 2006, **16**, 4413.
13 X. Wang, X. L. Wu, Y. G. Guo, Y. T. Zhong, X. Q. Cao, Y. Ma and J. N. Yao, *Adv. Funct. Mater.*, 2010, **20**, 1680.
14 W. M. Zhang, J. S. Hu, Y. G. Guo, S. F. Zheng, L. S. Zhong, W. G. Song and L. J. Wan, *Adv. Mater.*, 2008, **20**, 160.
15 J. Y. Wang, N. L. Yang, H. J. Tang, Z. H. Dong, Q. Jin, M. Yang, D. Kisailus, H. J. Zhao, Z. Y. Tang and D. Wang, *Angew. Chem. Int. Ed.*, 2013, **52**, 6417.
16 H. X. Yang, J. F. Qian, Z. X. Chen, X. P. Ai and Y. L. Cao, *J. Phys. Chem. C*, 2007, **111**, 14067.
17 L. Zhou, D. Y. Zhao and X. W. Lou, *Adv. Mater.*, 2012, **24**, 745.
18 Y. J. Hong, M. Y. Son and Y. C. Kang, *Adv. Mater.*, 2013, **25**, 2279.
19 H. L. Xu and W. Z. Wang, *Angew. Chem. Int. Ed.*, 2007, **46**, 1489.
20 X. Y. Lai, J. Li, B. A. Korgel, Z. H. Dong, Z. M. Li, F. B. Su, L. Du and D. Wang, *Angew. Chem. Int. Ed.*, 2011, **50**, 2738.
21 X. Y. Lai, J. E. Halpert and D. Wang, *Energy Environ. Sci.*, 2012, **5**, 5604.
22 Y. M. Chen, X. Y. Li, K. Park, J. Song, J. H. Hong, L. M. Zhou, Y. W. Mai, H. T. Huang and J. B. Goodenough, *J. Am. Chem. Soc.*, 2013, **135**, 16280.
23 Y. Wang, Z. S. Feng, C. Zhang, L. Yu, J. J. Chen, J. Hu and X. Z. Liu, *Nanoscale*, 2013, **5**, 3704.
24 C. F. Zhang, H. B. Wu, C. Z. Yuan, Z. P. Guo and X. W. Lou, *Angew. Chem. Int. Ed.*, 2012, **51**, 9592.
25 S. B. Yang, X. L. Feng, L. J. Zhi, Q. Cao, J. Maier and K. Müllen, *Adv. Mater.*, 2010, **22**, 838.
26 H. S. Zhou, S. M. Zhu and M. Hibino, *Adv. Mater.*, 2003, **15**, 2107.
27 Y. S. Hu, P. Adelhelm, B. M. Smarsly, S. Hore, M. Antonietti and J. Maier, *Adv. Funct. Mater.*, 2007, **17**, 1873.
28 Z. Sun, X. F. Song, P. Zhang and L. Gao, *RSC Adv.*, 2014, **4**, 20814.
29 X. J. Wu and D. S. Xu, *Adv. Mater.*, 2010, **22**, 1516.
30 S. Ikeda, K. Tachi, Y. H. Ng, Y. Ikoma, T. Sakata, H. Mori, T. Harada and M. Matsumura, *Chem. Mater.*, 2007, **19**, 4335.
31 X. Y. Wang, P. Wang, Z. H. Dong, Z. P. Dong, Z. Y. Ma, J. Jiang, R. Li and J. T. Ma, *Nanoscale Res Lett.*, 2010, **5**, 1468.
32 Y. Zhao, W. L. Wu, J. X. Li, Z. C. Xu and L. H. Guan, *Adv. Mater.*, 2014, **26**, 5113
33 G. He, S. Evers, X. Liang, M. Cuisinier, A. Garsuch and L. F. Nazar, *ACS Nano*, 2013, **7**, 10920.
34 H. S. Zhou, S. M. Zhu and M. Hibino, *Adv. Mater.*, 2003, **15**, 2107.
35 L. C. Liu, Q. Fan, C. Z. Sun, X. R. Gu, H. Li, F. Gao, Y. F. Chen and L. Dong, *J. Power Sources*, 2013, **221**, 141.
36 F. D. Han, Y. J. Bai, R. Liu, B. Yao, Y. X. Qi, N. Lun and J. X. Zhang, *Adv. Energy Mater.*, 2011, **1**, 798.
37 V. Subramanian, H. W. Zhu and B. Q. Wei, *J. Phys. Chem. B*, 2006, **110**, 7178.
38 M. Winter, J. O. Besenhard, M. E. Spahr and P. Novák, *Adv. Mater.*, 1998, **10**, 725.
39 N. A. Kaskhedikar and J. Maier, *Adv. Mater.*, 2009, **21**, 2664.
40 L. W. Ji and X. W. Zhang, *Nanotechnology*, 2009, **20**, 155705.
41 S. B. Yang, J. P. Huo, H. H. Song and X. H. Chen, *Electrochim. Acta*, 2008, **53**, 2238.
42 J. Y. Eom, D. Y. Kim and H. S. Kwon, *J. Power Sources*, 2006, **157**, 507.
43 N. S. Choi, Z. H. Chen, S. A. Freunberger, X. L. Ji, Y. K. Sun, K. Amine, G. Yushin, L. F. Nazar, J. Cho and P. G. Bruce, *Angew. Chem. Int. Ed.*, 2012, **51**, 9994.
44 X. W. Lou, C. M. Li and L. A. Archer, *Adv. Mater.*, 2009, **21**, 2536.
45 S. B. Yang, Y. J. Gong, Z. Liu, L. Zhan, D. P. Hashim, L. L. Ma, R. Vajtai and P. M. Ajayan, *Nano Lett.*, 2013, **13**, 1596.

A Table of contents entry:

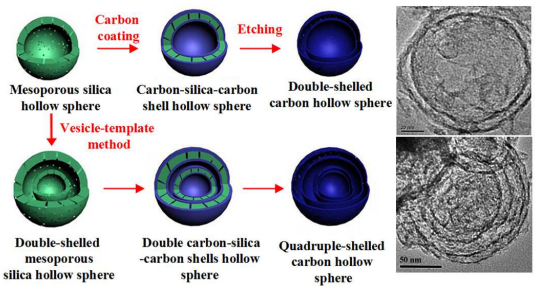

Double/quadruple shells carbon hollow spheres can be obtained under the assistance of permeably mesoporous silica hollow spheres, which exhibit superior electrochemical performance.